Est. 1984

ORIENTAL JOURNAL OF CHEMISTRY
An International Open Free Access, Peer Reviewed Research Journal

www.orientjchem.org

ISSN: 0970-020 X
CODEN: OJCHEG
2016, Vol. 32, No. (6):
Pg. 2939-2945

Synthesis and Investigation of Electrical Properties of Nanopowders Produced by Spark Erosion of Silver Electrodes in the Air

ALEXEY EFIMOV*, ANNA LIZUNOVA, IVAN VOLKOV, STEPAN LISOVSKII and VICTOR IVANOV

Department of Physical and Quantum Electronics,
Moscow Institute of Physics and Technology, Dolgoprudny, Russia.
*Correspondence author E-mail: efimov.aa@mipt.ru

http://dx.doi.org/10.13005/ojc/320613

(Received: October 13, 2016; Accepted: November 17, 2016)

ABSTRACT

The synthesis parameters and results of investigation of electrical properties of nanopowders produced by a spark erosion of silver electrodes in the air are presented. The powders are composed mostly of metallic silver (52.9 wt. %) and silver nitrate (46.5 wt. %) particles with the size less than 50 nm as determined from the transmission electron microscopy images and their specific surface area is ranging from 4 to 11 m^2/g. The powder production rate is estimated at 0.4 g/h. The corresponding particulate films demonstrated the ultimate resistivity of $3 \cdot 10^{-4}$ Ω·cm at room temperature.

Keywords: Silver nanopowder, Spark erosion, Aerosol, Printed electronics, Multi spark discharge generator.

INTRODUCTION

Functional nanoparticles are promising materials having a great potential of application in various technologies[1,2]. The spark discharge is a new challenging method for producing ultrafine particles with the size less than 10 nm directly in the gas phase: the synthesis of nanoparticles is accomplished through the spark erosion[3,4]. This method is quite simple and allows synthesizing versatile nanomaterials from parent bulk materials possessing satisfactory conductivity ($\rho < 0.2$ Ω cm)[5,6]; this condition is fulfilled for all metals and particular semiconductors such as doped Si, Ge, and Sb[3,5,7]. It is obvious that properties of nanoparticles synthesized by spark discharge depend on the purity of a carrier gas.[3,8] Keeping this in mind, one should use purified gases (e.g., Ar or He) to obtain chemically pure nanoparticles[3]. However, this approach increases significantly the powder production cost and, hence,

is used only for some special applications. Meanwhile, in such areas as air filter testing[9] and toxicological studies[10] of nanomaterials, it is quite enough to use air as a carrier gas. Therefore, the study of processes responsible for the synthesis of nanoparticles by spark erosion in the air is an urgent problem in cost-effective production of nanopowders.

In this paper, we present the results of investigation into the properties of nanoparticles produced by a spark erosion of silver electrodes in the air. The choice of silver is motivated due to the high demand of silver nanomaterials in printed electronics[11,12], photovoltaics[13] and medicine[14,15].

MATERIAL AND METHODS

The synthesis of aerosol nanoparticles through the spark discharge is implemented by using specially designed generators[16]. In this work, we used custom-built multi-spark discharge generator. A distinctive feature of this generator is a possibility of producing nanoparticles at high production rate (several grams per hour)[17]. This generator consists of 12 pairs of serially connected electrodes powered by 12 nF capacitor charged by high-voltage source (Fig. 1). The cylindrical electrodes made of pure silver (purity > 99.95%) with a nominal diameter of 6 mm are aligned axially at a distance of 0.5 mm (Fig. 1). The discharge is triggered by applying the voltage pulse to one of the central electrodes[18]. The source output voltage (4.5 kV) and the repetition rate (2.5 kHz) are tailored so that to enable the continuous operation of the generator in order to increase the long-term powder production rate. The electrodes are blown out continuously by the dry and clean air at a rate of 15 m/s. The energy released during the discharge leads to the erosion of electrodes with the subsequent formation of nanoparticles as a result of evaporation and condensation processes[19]. The airborne nanoparticles synthesized in the generator were deposited onto the filter made of porous stainless steel.

The powder production rate was estimated by weighing filter before and after the deposition. The crystal structure and phase composition of powders were studied by X-ray diffraction (XRD) with the use of Bruker D8 DISCOVER. The elemental composition was determined by inductively coupled plasma mass spectrometry (ICP-MS) with the use of Thermo Scientific iCAP Qc. The particle size distribution, morphological and structural features were investigated by transmission electron microscope (TEM) with the use of JEOL JEM-2100. The size distribution of as-synthesized airborne nanoparticles was measured by diffusional aerosol spectrometry with the use of AeroNanoTech DAS 2702. The specific surface area was determined by BET method with the use of Micromeritics TriStar 3000.

The electrical properties of synthesized powders were studied by four-terminal sensing with the use of Keithley 2401 instrument. For this purpose, the strips about 15 mm long and 1.5 mm wide were patterned on the surface of single-crystal sapphire substrates by screen printing. The pastes used for patterning were prepared by dispersing powders in the ethylene glycol. The fabricated samples were

Table 1: Results of XRD phase analysis of the powder produced by spark erosion of silver electrodes in the air

Phase	Lattice parameters, Å	Mean crystallite size, nm
Ag cubic (52.9 wt. %)	a = 4.087±0.002	36±2
$AgNO_3$ orthorhombic (46.5 wt. %)	a = 6.993±0.004 b = 7.329±0.004 c = 10.113±0.006	165±20
Ag_2O_3 orthorhombic (0.6 wt. %)	a = 13.690±0.008 b = 9.980±0.005 c = 3.669±0.005	> 200

annealed at various temperatures (up to 415°C) in air atmosphere with the use of IKA HS 7 hotplate. The measurements of the resistance were carried out at room temperature.

RESULT AND DISCUSSION

The powder production rate estimated at 0.4 g/h is few hundred times higher than that of conventional one-gap generators operating at low repetition rates (< 300 Hz)[3]. It was found from XRD phase analysis (Fig. 2) that the synthesized material contains the following crystalline phases: metallic Ag (52.9±0.5 wt. %), $AgNO_3$ (46.5±0.5 wt. %), Ag_2O_3 (0.6±0.1 wt. %). The results of XRD phase analysis, including lattice parameters and mean crystallite sizes are presented in the Table 1. It is straightforward to calculate from this data the total silver content (the fraction of silver in the overall mass of the material). Within the measurement accuracy, the calculated result (82.8±0.7 wt. %) converges with that found from ICP-MS analysis: 79±8 wt. %.

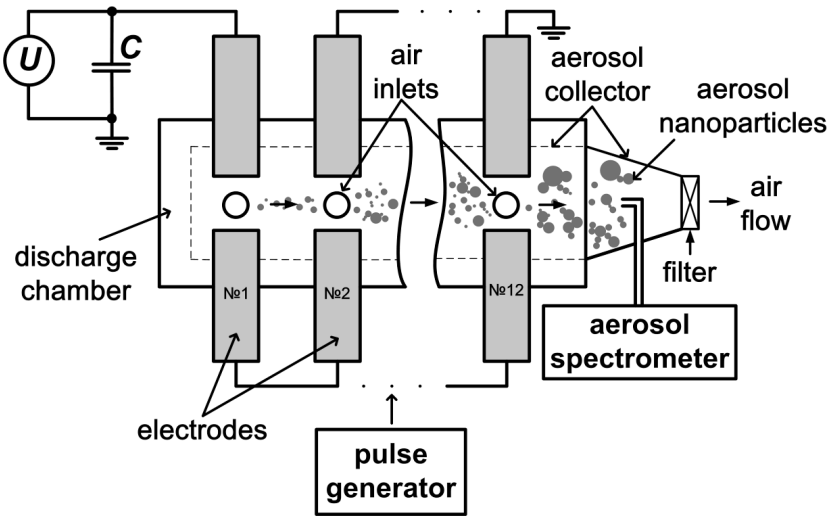

Fig. 1: A scheme of the multi-spark discharge generator

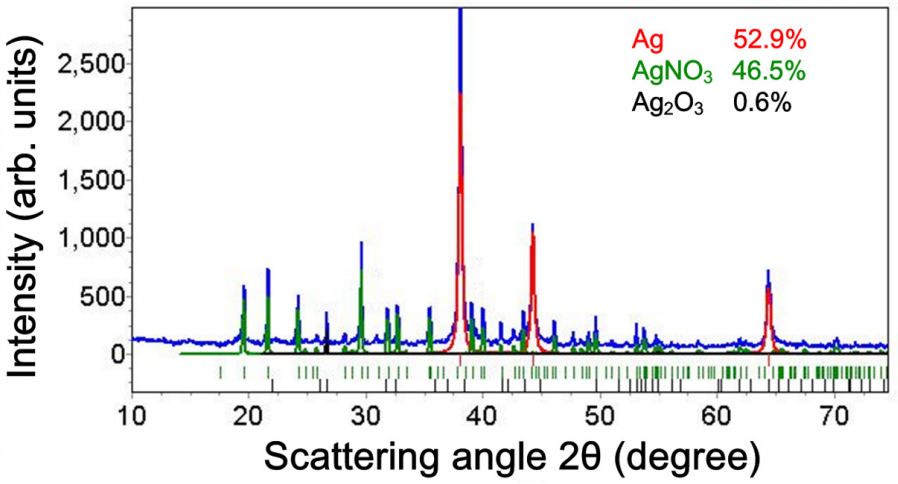

Fig. 2: Results of XRD phase analysis: the measured spectra are shown in blue, other spectra calculated by Rietveld method correspond to crystalline phases indicated in the upper right area of each figure

It can be assumed that the formation of silver nanoparticles is occurred via the condensation of vapors produced as a result of spark erosion of parent material, while the formation of silver nitrate and silver oxide nanoparticles is governed by the chemical reactions between the already formed silver nanoparticles and the gas-phase components of the carrier gas such as O_2, O_3, NO_x. The formation of $AgNO_3$ may proceed according to the following reaction:

$$Ag + 2NO_2 \rightarrow AgNO_3 + NO \quad (1)$$

The Ag_2O_3 is most likely formed as a result of the following reaction:

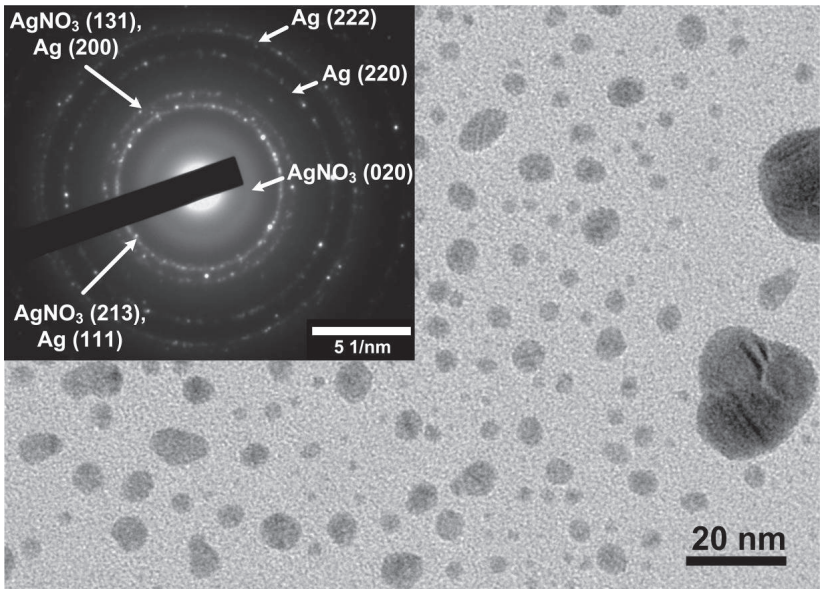

Fig. 3: TEM image of nanoparticles and corresponding electron diffraction pattern (inset)

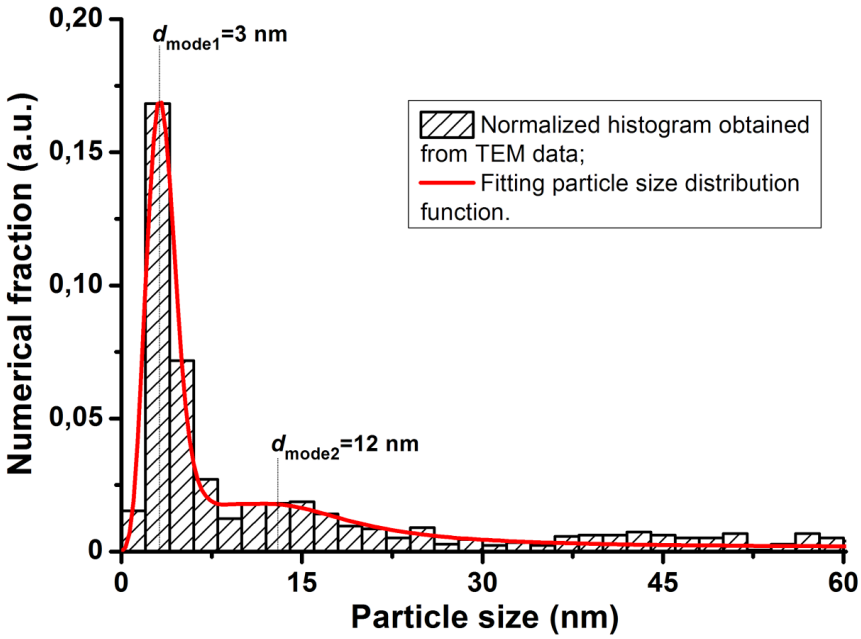

Fig. 4: Results of TEM analysis: normalized histogram and fitting function

$$4Ag + 3O_2 \rightarrow 2Ag_2O_3 \quad (2)$$

A typical TEM image of produced nanoparticles is shown in Fig. 3. The material consists of primary particles with different shapes, mostly of elliptical type. Here, the term primary refers to the smallest units of material formed in the close vicinity of the discharge zone. The aggregates containing several primary particles are also observed. The term aggregate refers to the assembly of primary particles connected through chemical bonds. The histogram obtained from the analysis of TEM images is well described by a superposition of two functions of log-normal distribution with modal sizes of about 3 and 12 nm, corresponding mostly to primary particles and its aggregates, respectively (Fig. 4). According to the electron diffraction pattern (inset of Fig. 3), the particles are crystalline; it is

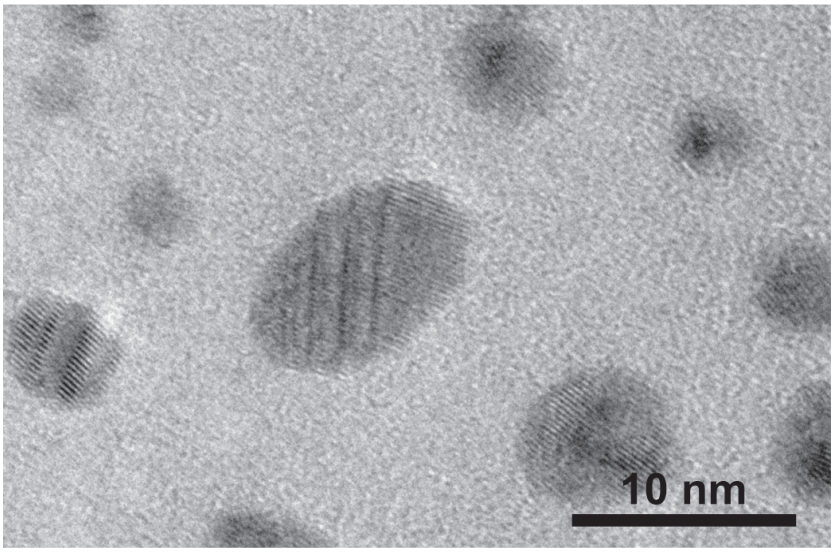

Fig. 5: TEM image of nanoparticles at high magnification

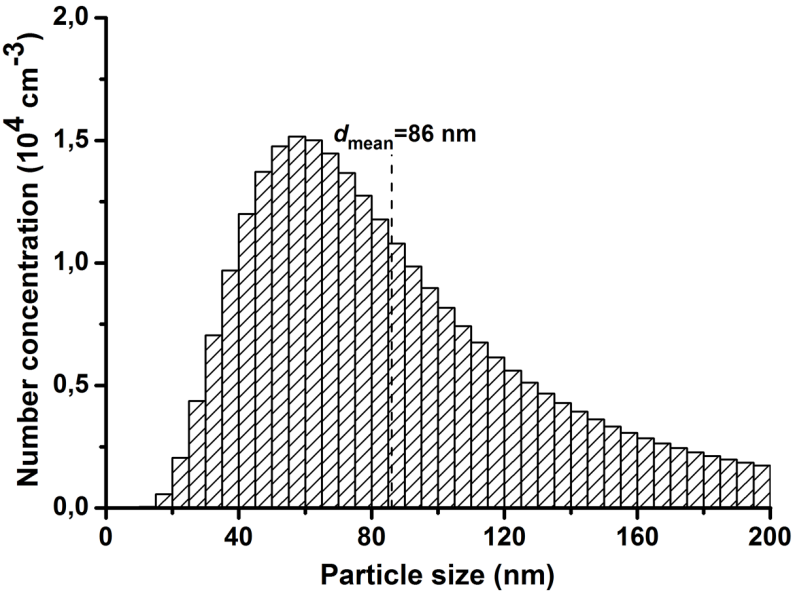

Fig. 6: Size distribution of as-synthesized airborne nanoparticles measured by diffusional aerosol spectrometry

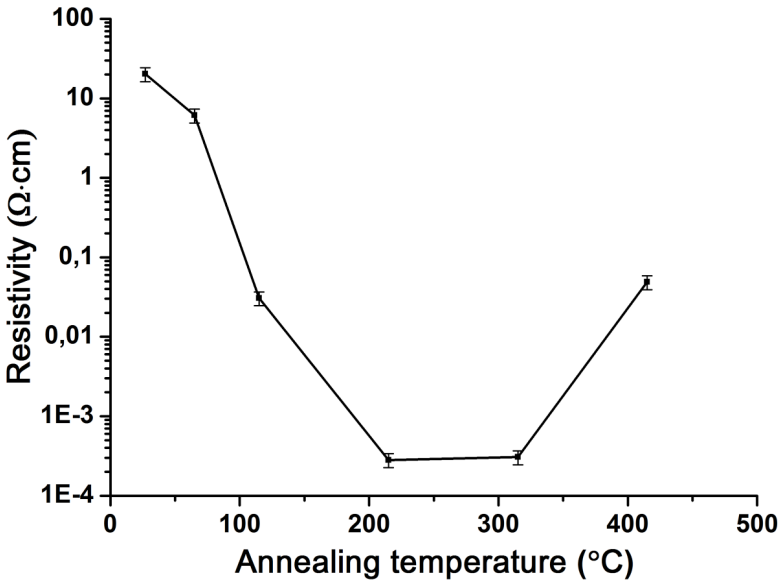

Fig. 7: Resistivity at 25°C of the particulate film prepared from the synthesized nanopowder as a function of annealing temperature

also evidenced by TEM images at high magnification (Fig. 5).

The particle size distribution of as-synthesized airborne particles is shown in Fig. 6. The distribution has one maximum located around 60 nm and the mean particle size is estimated to be 86 nm. The discrepancy between values of these statistical parameters obtained from TEM and aerosol analysis can be explained in terms of agglomeration of primary particles and its aggregates occurred in the gas phase during their transfer to the point of use (see Fig. 1). The specific surface area of a series of powders produced under the same synthesis conditions as determined by BET method is ranging from 4 to 11 m^2/g that corresponds to the equivalent particle size range from 52 to 143 nm; this result is in good agreement with the data obtained from the aerosol analysis (see Fig. 6), since both methods account for the particle agglomeration factor.

Figure 7 presents the typical dependence of a resistivity of the particulate film on the annealing temperature. The resistivity was calculated from the four-point resistance of a strip patterned on the surface of a single-crystal sapphire substrate, the distance between voltage contacts, and the cross sectional area of a strip. The last one was estimated from the stylus profilometry data.

The dramatic drop of the resistivity (about 4 orders of magnitude) in the temperature range up to 215°C can be explained by the evaporation of the residual ethylene glycol from the mesopores of a particulate film and the melting of the silver nitrate (Fig. 7). The first process causes particles to come closer to each other; as a result, the interparticle conductivity is increasing. In the second process, the silver nanoparticles (having greater density than silver nitrate) settle in the bulk of molten silver nitrate, thus forming highly conductive bottom layer. It should be noted that the melting point of nanostructured materials is lower than that of the bulk material of the same composition. In our case, the melting point of the major portion of silver nitrate is expected to be below 190°C.

The following increase in the annealing temperature (up to 315°C) has no effect on the resistivity. Finally, at elevated temperatures, the morphology of the particulate film is adversely affected by the substantial difference in the coefficients of linear thermal expansion of silver ($\sim 20 \cdot 10^{-6}$ K^{-1}) and sapphire ($\sim 7 \cdot 10^{-6}$ K^{-1}), thus

resulting in the noticeable increase in the resistivity. Therefore, the optimum annealing temperature is in the range 200–300°C. The ultimate resistivity of $3 \cdot 10^{-4}$ Ω·cm is about 190 times greater than that of bulk silver.

CONCLUSIONS

In conclusion, we have demonstrated the possibility of robust production of silver containing nanopowders in the air atmosphere at the production rate of 0.4 g/h with the use of multi-spark discharge generator. The synthesized materials contain 52.9 wt % of metallic silver composed of fine particles with the size less than 50 nm; the silver nitrate and to a much lesser extent the silver oxide account for the remaining 46.5 wt.%. The corresponding particulate films demonstrated the ultimate resistivity of $3 \cdot 10^{-4}$ Ω cm at room temperature which is suitable for a number of electronic applications (for example, as microheaters and interconnectors).

ACKNOWLEDGEMENTS

This work was supported by the Russian Science Foundation (project # 15-19-00190).

REFERENCES

1. Kruis, F. E.; Fissan, H.; Peled, A. *J. Aerosol Sci.* **1998**, *29*, 511–535.
2. Yadollahpour, A.; Rashidi, S. *Orient. J. Chem.* **2015**, *31*, 25–30.
3. Tabrizi, N. S.; Ullmann, M.; Vons, V. A.; Lafont, U.; Schmidt-Ott, A. *J. Nanoparticle Res.* **2009**, *11*, 315–332.
4. Efimov, A.; Sukharev, V.; Ivanov, V.; Lizunova, A. *Orient. J. Chem.* **2015**, *31*.
5. Vons, V. A.; Smet, L. C. P. M. de; Munao, D.; Evirgen, A.; Kelder, E. M.; Schmidt-Ott, A. *J. Nanoparticle Res.* **2011**, *13*, 4867–4879.
6. Efimov, A.; Lizunova, A.; Sukharev, V.; Ivanov, V. *Korean J. Mater. Res.* **2016**, *26*, 123–129.
7. Kala, S.; Rouenhoff, M.; Theissmann, R.; Kruis, F. E. In *Nanoparticles from the Gasphase*; Lorke, A.; Winterer, M.; Schmechel, R.; Schulz, C., Eds.; NanoScience and Technology; Springer Berlin Heidelberg, **2012;**. 99–119.
8. Vons, V. A.; Anastasopol, A.; Legerstee, W. J.; Mulder, F. M.; Eijt, S. W. H.; Schmidt-Ott, A. *Acta Mater.* **2011**, *59*, 3070–3080.
9. Efimov, A. A.; Ivanov, V. V.; Volkov, I. A.; Subbotina, I. R.; Pershin, N. A. *Nanotechnologies Russ.* **2013**, *8*, 789–798.
10. Jing, X.; Park, J. H.; Peters, T. M.; Thorne, P. S. *Toxicol. Vitro Int. J. Publ. Assoc. BIBRA* **2015**, *29*, 502–511.
11. Periasamy, V.; Ciniciato, G. P. M. K.; Yunus, K.; Fisher, A. C. *Appl. Phys. Express* **2015**, *8*, 27002.
12. Zhao, D.; Liu, T.; Park, J. G.; Zhang, M.; Chen, J.-M.; Wang, B. *Microelectron. Eng.* **2012**, *96*, 71–75.
13. Mizuno, H.; Sai, H.; Matsubara, K.; Takato, H.; Kondo, M. *Appl. Phys. Express* **2014**, *7*, 112302.
14. Chen, X.; Schluesener, H. J. *Toxicol. Lett.* **2008**, *176*, 1–12.
15. Thakur, A.; Reddy, S. G. *Orient. J. Chem.* **2016**, *32*, 1465–1472.
16. Meuller, B. O.; Messing, M. E.; Engberg, D. L. J.; Jansson, A. M.; Johansson, L. I. M.; Norlén, S. M.; Tureson, N.; Deppert, K. *Aerosol Sci. Technol.* **2012**, *46*, 1256–1270.
17. Ivanov, V. V.; Efimov, A. A.; Mylnikov, D. A.; Lizunova, A. A.; Bagazeev, A. V.; Beketov, I. V.; Shcherbinin, S. V. *Tech. Phys. Lett.* **2016**, *42*, 876–878.
18. Mesyats, G. A. *Pulsed Power*; Springer Science & Business Media, **2007**.
19. Feng, J.; Biskos, G.; Schmidt-Ott, A. *Sci. Rep.* **2015**, *5*, 15788.